Residual Stresses in the Porcelain Veneer Layer of All-Ceramic Restorations

Thomas Suranyi, DDS

A thesis submitted to the faculty of the University of North Carolina at Chapel Hill in partial fulfillment of the requirements for the degree of Master of Oral Biology in the School of Dentistry (Prosthodontics).

Chapel Hill
2011

Approved by:

David Felton, DDS MS

Lyndon Cooper, DDS PhD

Terry Donovan, DDS

ABSTRACT

Thomas Suranyi, DDS: Residual Stresses in the Porcelain Veneer Layer of All-Ceramic Restorations
(Under the direction of Drs. David Felton, Lyndon Cooper & Terry Donovan)

Objectives: Literature evidence suggests that chipping of the porcelain veneer layer in zirconia based all-ceramic restorations is greater when compared to porcelain fused to metal restorations. The aims of this study were to determine, *in vitro*, what roles rapid cooling and thermal diffusivity had on chipping and to determine whether failure mechanisms *in vitro* were comparable to those found *in vivo*. **Methods & Materials:** CAD/CAM was used for sample fabrication, with subsequent static and dynamic loading. Specimens were fractographically evaluated. **Results:** Quantitative analysis revealed higher residual stress in rapidly cooled samples. Fractographic analysis of *in vitro* samples demonstrated origins of failure and directions of crack propagation stemming from sites adjacent to load application. **Conclusion:** Samples rapidly cooled were found to have had larger chipping of the veneer layer. The findings of this study demonstrate inconsistent failure mechanisms between laboratory samples and published reports of failure mechanisms found *in situ.*

TABLE OF CONTENTS

LIST OF TABLES

Table

LIST OF FIGURES

Figure

LIST OF ABBREVIATIONS

Abbreviations

CAD	Computer Aided Design
CAM	Computer Aided Manufacturing
DPRP	Direct Pressing Resin Pattern
E_k	Kinetic Energy
FT	Fatigue Testing
PFM	Porcelain Fused to Metal
SEM	Scanning Electron Microscopy
SLF	Single Load to Failure
ZBAC	Zirconia Based All-Ceramic

INTRODUCTION

In light of the favorable aesthetic and biocompatible nature of Zirconia based all-ceramic restorations (ZBAC), chipping of the porcelain veneer layer is found to be higher when compared to porcelain fused to metal restorations. With a continued and growing demand for aesthetic restorations, determining the causes of ZBAC restoration veneer chipping will improve the prognosis for esthetically driven oral rehabilitations relying on all-ceramic systems. It is our endeavor to determine what roles heating/cooling rates and thermal diffusivity play in ZBAC restoration failure.

The advent of CAD/CAM and additive manufacturing technologies has simplified the process of fabricating all-ceramic restorations. Rapid prototyping technologies can eliminate many variables in the mutli-step process of making a simple restoration such as a crown. This study will use both milling and 3D printing in effort to fabricate dimensionally accurate test samples.

The aims of this study are to: (1) determine what role the interaction between the thermal diffusivities of zirconia and porcelain play in veneer chipping, (2) The feasibility of using rapid prototype technologies in the fabrication of simple restorations and (3) to determine how failure mechanisms *in vitro* compare to failure mechanism *in vivo*.

Chapter 1

Residual Stresses in the Porcelain Veneer Layer of All-Ceramic Restorations

Introduction

Zirconia Based All-Ceramic (ZBAC) Restorations

With the advent of computer aided design/computer aided manufacturing (CAD/CAM) technology and the introduction of ZBAC restorations, fabrication of a fixed prosthesis has been simplified[5]. In comparison with porcelain fused to metal (PFM) restorations the total number of steps in fabricating fixed restorations has been reduced[1]. Milling of ZBAC restoration copings has the benefit of producing predictable and consistent substructures in terms of strength, marginal fit, and esthetics. Additionally, this technique is less labor intensive than waxing and casting traditionally used for PFM restorations. In terms of veneering porcelain, the use of zirconium oxide has allowed for fewer sintering steps in comparison with PFM restorations, thus increasing workflow. Zirconia shades eliminate the need for opaque layers, which require one to two applications.[2] Likewise, PFM restorations with porcelain butt-joints require additional application of shoulder porcelain, typically two applications.[3] Not until the application of

dentin porcelains do ZBAC and PFM restorations become similar in the number of steps required for completion. At that juncture the application of dentin, effect powders and enamel porcelains are virtually identical.

In Vivo Literature Data on Porcelain Chipping During Clinical Function

Veneer chipping in ZBAC restorations is well documented in the dental literature (Table 1.1 expanded from Al-Amleh 2010).[4,5] Among the 22 clinical trials listed, the longest follow up period was 5 years and the shortest 1 year. Both single unit and fixed partial dentures were evaluated. Sample sizes varied from 13 to 204.

As the popularity of all-ceramic systems continues to grow efforts to determine etiologies for failure in ZBAC restorations continue[6]. The likelihood of practitioners and dental laboratories accepting new rapid prototyping technologies, such as those involved in the fabrication of ZBAC restorations, is, among other factors, associated with clinical success[7].

Coefficient of Thermal Expansion, Thermal Diffusivity & Glass Transition Temperature

The use of low crystalline dental porcelains for veneering of high crystalline metal-oxide ceramics has important material implications, including the interplay between the coefficients of thermal expansion (CTE), thermal diffusivities (TD) and glass

transition temperatures (Tg)[8]. The manner in which these material properties interact during the sintering process of ZBAC restorations may lead to porcelain chipping[9].

Table 1.1: In vivo Trials of Zirconia Based All-Ceramic Restorations

Brand	Study	Period (yr)	Restorations	Sample (crowns or FPDs)	Framework Fracture (%)	Debonding (
Cercon Zr (Dentsply)	Sailer et al.2007	5	3-5 unit FDP	33	8	15
	Beuer et al.2009	3	3 unit FDP	21	5	0
	Cehreli et al.2009	2	Single Crowns	15	7	0
	Schimitter et al.2009	2	4-7 unit FDP	30	3	3
	Bornemann et al.2003	1.5	3-4 unit FDP	59	0	3
LAVA (3M ESPE)	Raigrodski et al.2006	2.5	3 unit FDP	20	0	25
	Pospiech et al.2003	2	3 unit FDP	38	0	3
	Schmitt et al.2010	3	Single ant crowns	19	NA	5.3
	Crisp et al.2008	1	3-4 unit FDP	38	0	3
Procera Zr (Nobel Biocare)	Ortrop et al.2009	3	Single crowns	204	0	2
IPS e.max Zir/CAD (Vivadent-Ivoclar)	Ohlmann et al.2008	1	IRFDP	30	10	13
Denzir (Cadesthetics AB)	Molin & Karlsson 2008	5	3 unit FDP	19	0	36
	Larsson et al.2006	1	2-5 unit FDP/Ti Abut	13	0	54
DC-Zirkon (DCS Dental AG)	Tinschert et al.2008	3	3-10 +cantilever	65	0	6
	Vult von Steyern et al.2005	2	3-5 units FDP	23	0	15
Digizon	Edelhoff et al.2008	3	3-6 units FDP	21	0	9.5
In-Ceram Zirconia (Vita Zahnfabrik)	Eschbach et al. 2009	4.5	3 unit FDP Post	65	1.5	6.3
Cercon (DeguDent)	Larsson et al.2010	3	9-10 unit full arch	10	0	34
	Roediger et al.2010	4	3-4 unit FDP	75	1.1	19.6E/8.9C
	Sailer et al. 2009	3	3-5 unit FDP	38Z/38M	0	25Z/19.6M
Cercon(?) (DeguDent)	Wolfart et al. 2009	4	3-4 unit cantilever	107	0	13C/12T
Nanozir, Hint-Els	Sailer et al 2010	1	3	8	0	0

FDP, Fixed dental prosthesis; IRFDP, Inlay-retained fixed dental prosthetis; E, experimental; C, control; Z, zirconia; M, metal; T, Test

Coefficient of Thermal Expansion (CTE)

At a given temperature, atoms have a degree of kinetic energy (E_k). In crystalline and non-crystalline ceramic restorations this E_k is governed by the input and withdrawal

of heat. The higher the heat input the higher the kinetic motion, or vibration, of an atom or molecule. This higher amplitude of vibration results in a greater interatomic space. This is recognized as thermal expansion (K^{-1}), and is calculated as follows[8,10]:

$$\text{CTE} = \frac{\text{Length final} - \text{length orginal}}{\text{length original X } (^{\circ}\text{Cfinal} - ^{\circ}\text{Coriginal})}$$

Materials exhibit greater or lesser degrees of expansion. In metal-ceramic restorations, this has led to the use of veneering porcelains with a slightly lower CTE than the supporting metal substructure. In doing so, compressive stresses in the veneering porcelain are generated on the metal coping.[11] Ceramic veneer layers may fracture if their thermal coefficients are greater than that of its metal substructure.[2] As such; the CTE interplay between veneering porcelain and coping has been an important factor in the development of porcelain systems.

Thermal Diffusivity (TD)

CTE is influenced by a material's thermal diffusivity (m^2/s) which is defined as[8]:

$$\alpha = k/\rho \cdot Cp$$

Where α is thermal diffusivity (m^2/sec), k is thermal conductivity (W/m·K), ρ is density (kg/m^3) and Cp is specific heat capacity (J/kg·K). Materials with a high α are efficient diffusers of thermal energy and vice versa.[12] This equation allows us to

understand how a material's ability to conduct energy, its thermal conductivity (k), relates to its ability to store energy without undergoing a phase transformation over a range of temperatures, a property known as heat capacity ($\rho \cdot Cp$). As such, the CTE is affected by a materials ability to absorb and release heat: in effect, α influences CTE. In terms of dental restorations, no universal value for thermal diffusivity is recognized as ideal. However, core and veneer should have compatible thermal diffusivities.

Glass Transition Temperature (Tg)

A crystalline structure has a well organized lattice with repeating unit cells. Non-crystalline structures tend to be amorphous with no, or little, organization. When either of these materials is heated, they lose their lattice structure and exhibit properties more akin to liquids. Conversely, as these materials are cooled and their basic unit cells re-organize there is a sudden decrease in CTE. The temperature at which this occurs is known as the glass transition temperature (Tg)[8]. Below Tg a material loses its fluid characteristics and develops an increased resistance to shear forces. In effect, below Tg dental porcelains and zirconia copings are solids, resistant to deformation.

Interplay of CTE, TD & Tg

How may CTE, TD and Tg play a role in veneer chipping in ZBAC restorations? Zirconia is an excellent insulating agent as compared to veneering porcelains (TD Y-TZP 0.74 X 10^{-6} m^2s^{-1}, porcelain 1.0 X 10^{-6} m^2s^1)[10,13,14,15]. As such, while their CTEs are

compatible, their thermal diffusivities are not. Therefore, when ZBAC restorations are placed in a sintering or press furnace, differential heat absorption takes place between the veneer and coping. Zirconia's TD is lower than that of porcelain and during the sintering cycle's cooling phase it releases its heat at a slower rate. The consequence is that the veneering layer cools and reaches its Tg before the zirconia substructure. While the veneer layer has established its crystalline lattice, the zirconia coping continues to cool and contract placing tensile stress in the overlaying porcelain. It is theorized that during function this pre-stressed state is relieved in the form of veneer debonding[15,16].

Study Aims

The first aim of this study is to determine whether post-pressing rapid cooling of ZBAC restorations can accentuate the pre-stressed state, thus leading to greater failure intensity on loading. The null hypothesis is that rapidly cooled restorations will have less resistance to failure on loading in the laboratory environment.

The second aim is to determine what effect increasing the coping thickness from 0.3 to 0.5 mm will have on load resistance.[15] The null hypothesis is that by increasing coping thickness it will lower the thermal diffusivity (increased mass leads to lower thermal diffusivity), thereby leading to less resistance to failure on loading in the laboratory environment.

Materials & Methods

Rapid prototyping technologies can eliminate many variables in the multi-step process of making a simple restoration such as a crown. Consequently, dies, copings and direct pressing resin patterns (DPRP) were designed and modeled with the use of CAD/CAM and 3D printing (Figure 1).

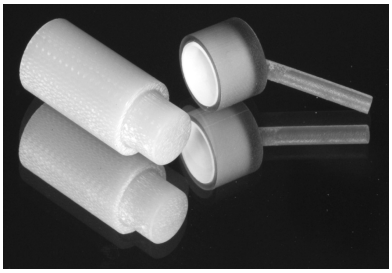

Figure 1. Die, DPRP with coping
(Note sprue on occlusal surface)

Dies

3D CAD software, SolidWorks® (Dassault Systemes Solidworks Corp., Concord, MA), was used to design dies with the following dimensions (Figure 2, Table 1.2):

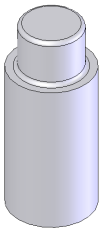

Figure 2. Die

Table 1.2: Die Dimensions

Parameter	Length(mm)
Total Height	25.05
Base Height	19.05
Core Height	6.0
Core Diameter	8.0
Total Diameter	11.0
Should Width	1.5
Occluso-Axial Bevel	0.5
Axial Wall Taper	0^0 (degree)
Axio-Gingival Bevel	0.5

Core height and shoulder width were loosely modeled on average dimensions of a prepared mandibular first molar for an all-ceramic restoration[17]. A continuously woven glass fabric epoxy resin laminate (National Electrical Manufacturers Association (NEMA) grade G10, Rosslyn, VA), was used as a milling substrate and has previously been reported in laboratory use[18,19]. Axio-occlusal/gingival line angles were beveled 0.5 mm in order to prevent stress concentrations.

Copings

Table 1.3 outlines group divisions, the number of samples in each group, the coping thicknesses, and the geometry of each sample. Each of these coping groups were subsequently pressed with porcelain and further categorized by coping thickness and cooling rate (Table 1.6).

Table 1.3: Lava™ Groups, Coping Thicknesses & Geometry

Groups	#/group	Coping Thickness (mm)	Geometry
S.3	10	0.3	Cylindrical
F.5	10	0.3	Cylindrical
S.3	10	0.5	Cylindrical
F.5	10	0.5	Cylindrical

Non-anatomic, cylindrically shaped designs were used in order to prevent non-uniform stress distribution[20,21]. Previous publications have shown that this geometry may be used to confirm residual stresses in bilayered ceramic systems[22,23]. The cylindrical shape should not be misconstrued as a standard crown.

Direct Pressing Resin Patterns (DPRP)

DPRPs were used for application of IPS e.max Zirpress (Ivoclar Vivadent, Amherst, NY), in a manner similar to the lost wax technique (Figure 3), to LAVA™ zirconia (3M ESPE, St. Paul, MN) copings.[24] Clear IPS e.max Ceram Zirliner (Ivoclar Vivadent, Amherst, NY) was applied to each coping, with firing and pressing guidelines obtained from the IPS e.max Zirpress Instructions for Use Manual (Table 1.4). High translucency, shade A1 IPS e.max Zirpress (Ivoclar Vivadent, Amherst, NY), ingots were used in order to facilitate optical imaging for subsequent fractographic analysis of failed restorations.

Figure 3. DPRP (Note sprue from occlusal)

DPRPs were designed on SolidWorks® (Dassault Systemes Solidworks Corp., Concord, MA) and printed (Invision HR, 3D Systems Rock Hill, SC) using Visijet SR200 Blue (3D Systems, Rock Hill, SC). Resin patterns were designed to apply 1.75 mm of occlusal and 1.5 mm of axial porcelain, dimensions previously modeled for determining residual stress in bilayered ceramic systems.[17,23] 40 DPRPs were printed, half to accommodate coping thicknesses of 0.3 mm and half for 0.5 mm. These dimensions are commonly used in the fabrication of ZBAC restorations.

Table 1.4: Press/Firing Parameters for IPS e.max*

IPS e.max	B (□C/□F)	S (min)	t↗ (□C/□F)	T (□C/□F)	H (min)	V_1 (□C/□F)	V_2 (□C/□F)
ZirLiner	403/757	4:00	60/108	960/1760	1:00	450/842	959/1758
ZirPress (200g)	700/1292	n/a	60/108	910/1670	15	500/932	910/1670
Glaze	403/757	6:00	60/108	770/1418	1:00-2:00	450/842	769/1416

***Table 1.5: Legend for Table 1.4**

Porcelain Firing Table Parameter	Symbol
Start Temperature (^{0}C or ^{o}T)	B
Dry Time (min)	S
Temperature Rise	T
Final Temperature	T
Hold Time	H
Vacuum Engage	V_1
Vacuum Disengage	V_2

Clear IPS e.max glaze (Ivoclar Vivadent, Amherst, NY) was applied to each sample and fired according to the manufacturer's recommendations (Table 1.4). Crowns were cemented with RelyX Luting Cement (3M ESPE, Germany) and aged in water for 30 days at 37°C in an incubator. Aging in this manner allowed for chemically assisted crack growth[25].

Cooling Rates

Cooling rates, coping thicknesses, veneer thicknesses and time to handling are outlined below (Table 1.6). Groups S.3 and S.5 underwent cooling according to the manufacturer's recommendations; time to handling was, on average, 53 minutes; calculated from completion of press cycle (EP 6000 Combi, Ivoclar Vivadent, Amherst, NY) to divesting of samples. Groups F.3 and F.5 underwent fast cooling with the use of compressed room temperature air. Once removed from the furnace (EP 6000 Combi, Ivoclar Vivadent, Amherst, NY) each sample was placed 12 inches from a fan and rotated

180 degrees every 5 minutes until handling was possible. The average time to handling was, on average, 17 minutes.

Table 1.6: Coping/Porcelain Veneer Thickness & Heating Rates

Groups (10/grp)	Cooling Rate	Coping Thickness (mm)	Occlusal/Axial Porcelain Thickness (mm)	Average Time to Handling (min)
S.3	MR	0.3	1.75/1.5	53
F.3	F	0.3	1.75/1.5	17
S.5	MR	0.5	1.75/1.5	53
F.5	F	0.5	1.75/1.5	17

MR= Manufacturer Recommended; F=Fast

Loading

Samples were placed in a universal testing machine (Model 5566 Instron, Acton, MA, USA) and all data values recorded in Newton force.[26] Forces were applied through a 6.25 mm radius tungsten carbide indenter at a rate of 1 mm/min (see figure 4). Each sample was loaded at the same location as shown in Figure 4. A guide was fabricated and the occlusal surfaces marked to ensure indenter application at the same radius.

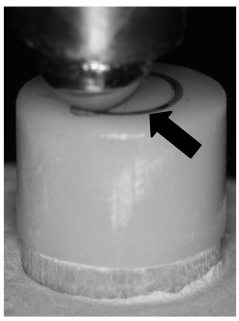

Figure 4. Samples loaded on occlusal. Contact point confined within black ring (arrow)

Subsequent analysis under visual and stereomicroscope evaluation (MZ APO, Leica Microsystems Inc. Bannockburn, IL, USA) was completed. Each failed sample was viewed with the naked eye and subsequently placed under 6.3X, 10X, and 20X magnifications. The surfaces were evaluated to determine areas and magnitude of failure. Direct comparison of samples within and among groups was undertaken.

Statistical Analysis

Two explanatory variables exist within each group of 10 samples. A factorial ANOVA with main effect and interaction was used to test the hypothesis. The assumptions are: interval data of the dependent variable, multivariate normality, homoscedasticity, and no multicollinearity.

Results

Statistical Analysis Results

Cooling rate and coping thickness were both represented in the categorical variable group as S.3, F.3, S.5, and F.5. To test for interaction, two categorical variables were created based on the values of variable group—one designated for values of cooling rate (variable cooling), and another designated for values of coping thickness (variable thickness). There were two coping thickness values, for each value there were two cooling values, and for each of the four cells or combinations of these two variables, there were ten values (force at failure), giving a total of 40 load values. See tables 1.7 and 1.8 for summary statistics of force and summary for two way factorial ANOVA analysis.

Table 1.7: Summary Statistics of Force (Newton) at Failure for Each Group

Group	N	Mean	Std Dev	Minimum	Maximum
S.3	10	1843.9	677.4	521.4	2726.4
F.5	10	1897.8	587.2	820.4	2997.0
S.5	10	1804.7	479.5	800.5	2608.4
F.5	10	1972.8	319.5	1497.5	2606.8

Table 1.8: Two-Way Factorial ANOVA: Dependent Variable = Load (Force at Failure; Newton)

Source	DF	Sum of Squares	Mean Square	F Value	Pr > F
Model	3	158978.3	52992.7	0.19	0.905
Error	36	10220435.0	283900.9		
Corrected Total	39	10379413.3			
R-Square	Coeff Var	Root MSE	Load Mean		
0.015317	28.3	532.8	1879.8		
Source	DF	ANOVA SS	Mean Square	F Value	Pr>F
Cooling	1	3185.3	3185.3	0.01	0.916
Thickness	1	123208.9	123208.9	0.43	0.514
Cooling Thickness	1	32584.1	32584.1	0.11	0.737

For the interaction hypothesis (see table 1.8) the test statistic F=0.11 with p=0.737, the conclusion is that there is no statistically significant interaction between cooling rate and coping thickness on force at failure. For cooling, the test statistic F=0.01 with p=0.916, the conclusion is that the average force at failure is not statistically significantly different for the two cooling rates. For coping thickness, the test statistic F=0.43 with p=0.514, the conclusion is that the average force at failure is not statistically significantly different for the two coping thicknesses.

Visual Display for Descriptive Statistics for Load to Failure (Newton) Separated by Group

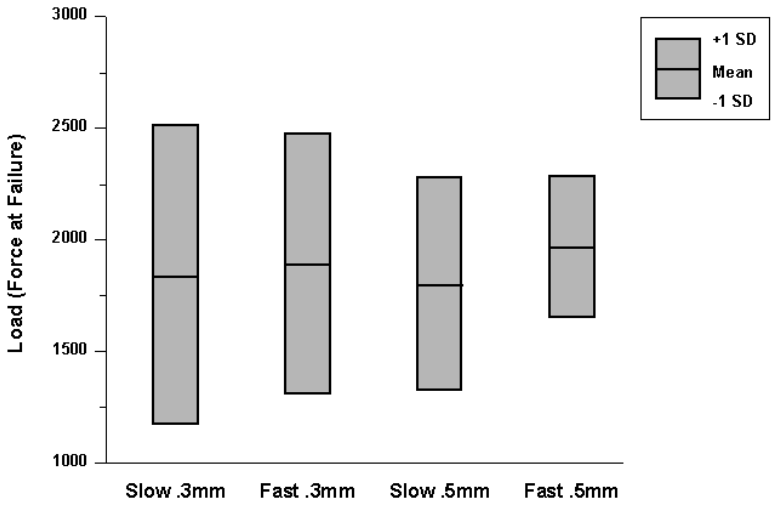

Sample Analysis

Visual and stereomicroscopic evaluation (figure 5) of failed laboratory samples revealed veneer chipping in all groups confined to the veneer layer. On average chipping occurred with higher intensity in groups F.3 and F.5. Groups S.5 & F.5 demonstrated

similar fracture patterns. None of the 40 samples tested had failure involving the zirconia core. Increasing coping thickness, thereby decreasing thermal diffusivity, had no apparent influence on force at failure or extent of veneer chipping.

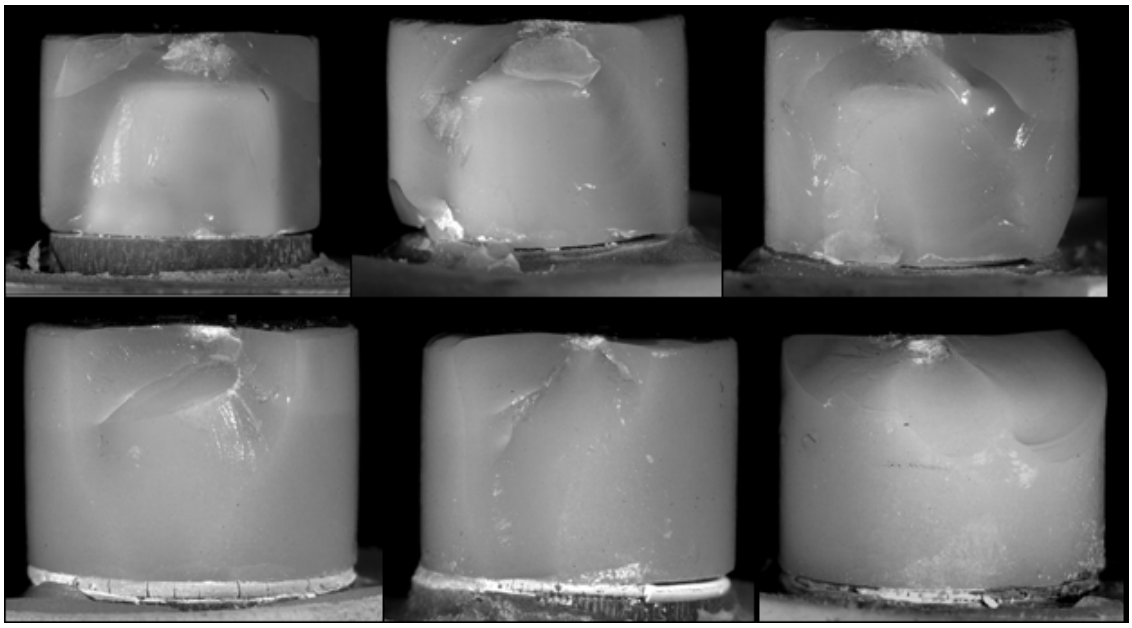

Figure 5. Top row: 3 representative samples from F.3 (fast cooled) cohort. Bottom row: 3 representative samples from S.3 (cooled according to the manufacturer's recommendation) cohort. Note larger chipping in the fast cooled group (magnification 10X).

Discussion

Interpretation of Optical Microscopic Evaluation of Failed Samples

What was noted with regard to the failure intensity of the two sample sets seen in figure 5? The answer is determined by quantitative analysis and in this case centers on visual inspection and light stereomicroscopic evaluation of samples within each group. Quantitative analysis makes an estimate of residual stress at failure[18]. There are four types of quantitative analysis: fragment analysis, branching distance analyses, fracture mirror size analysis and origin size analysis. Fragment analysis allows for the determination of net residual stress at failure, and therefore is the choice method for analysis.

With regard to fragment analysis, it has been stated that the lower the stress state at failure, the smaller the fragment size[27,28]. The net stress (αnet) at time of failure is governed by the following equation[29]:

$$\alpha_{net} = \alpha_a + \alpha_r$$

Where αa is the applied stress, and αr is the post fabrication residual stress in the veneer layer. Applied and residual stresses may be additive or subtractive. With the inherent residual compressive stresses in veneer layers on metal ceramic restorations αr is subtractive and reduces αnet, thereby increasing resistance to failure. When αr is

additive, as seen in the test samples during this study, it increases αnet, thereby resulting in larger chips. Statistical analysis showed that there was no difference in terms of the force at failure between groups; therefore, αa is considered a constant and the net stress at failure becomes proportional to the residual stress (αr). When applying this concept to the larger chips seen in figure 5, the question became which samples, those cooled according to the manufacturer's recommendation or those fast cooled had higher additive αr? The samples fast cooled demonstrated larger chipping and therefore proved to have a higher net stress at failure.

Varying Volumetric Heat Capacity

On visual inspection and light microscopic evaluation it was concluded that varying the volumetric heat capacity (ρ·Cp) had no effect on load resistance or degree of veneer chipping.

Previously Published Reports on Residual Stresses in Bilayered Systems

Swain MV has provided a theoretical background for the effects of residual stresses in bi-layered ceramic systems.[15] He considered the effects of thermal expansion mismatch, thermal conductivity, magnitude of thermal tempering, contact-induced fracture of thermally tempered plates and cooling rates on residual stresses of ceramic systems. In ZBAC restorations it was shown that the difference in thermal diffusivity

between veneering porcelain and zirconia substructure resulted in high residual stresses. Thermal expansion has not typically been a factor for residual stresses in these systems due to the similar CTEs of the materials used. It has been shown, *in vitro*, that cooling plays a role in degree of residual stress[23]. With the use of spherical models, Guazzato M was able to demonstrate the impact firing protocols have on spontaneous fractures among different veneering porcelains.[23] It was shown that extending cooling times and modifying cooling rates reduced the number of spontaneous fractures seen in test specimens. The results of this study confirm that increasing the heating/cooling rate results in greater residual stress within the veneer layer. Findings in this study are, therefore, congruent with previously published reports.

In Vivo vs In Vitro

Ideally, the results obtained in this study would be clinically correlated and inferences made regarding possible changes to fabrication methods of ZBAC restorations to reduce chipping rates. Unfortunately, no mode of correlation exists and developing stress states in laboratory samples identical to those found in the oral cavity is not currently feasible. The question at hand has been an age old debate: what is the clinical significance of laboratory data? *In vitro* data pertains more to determining physical properties of materials than predicting clinical performance[22,31]. The debate over laboratory studies typically intensifies when claims are made that samples tested in the laboratory environment can predict clinical outcome[23]. Traditionally, dental materials have been introduced for clinical use based on physical properties and adherence to

standards established by the American Dental Association and the International Organization for Standardization (ISO). However, no correlation exists between standards established by these organizations and clinical behavior. Ultimately, beyond basic tests for physical properties, only the data obtained from long term clinical studies present applicable information for clinical practice[23,32].

Study Limitations

The sizes of the chips in the veneer layers were not measured after failure. This information may have provided more detail regarding the degree of residual stress. Likewise, coping thicknesses were increased from 0.3 to 0.5mm, however the actual numerical decrease in thermal diffusivity was not determined. There may not have been an appreciable difference.

Conclusion

The following conclusions were drawn from the laboratory data obtained:

1. Rapid cooling of ZBAC restorations increases failure intensity on loading (based on quantitative analysis), however no effect was noted in terms of load resistance.
2. Decreasing thermal diffusivity, by increasing coping thickness, had no bearing on load resistance or failure intensity (based on quantitative analysis).
3. No mode of correlation currently exists for translation of laboratory data to the clinical arena.
4. The null hypotheses were rejected.

Chapter 2

Fractographic Analysis of Failed All-Ceramic Restorations: In Vivo vs In Vitro

Introduction

Restorations fail for one of three reasons: a design flaw, a material deficiency or *in vivo* stress-induced conditions[34]. Based on fractographic analysis of clinically failed restorations, it is possible to define and analyze the events leading to failure. Several reports of fractographically analyzed crowns have revealed differing etiologies for clinical failure (see Table 2.1).

In a case report of two clinically failed restorations it was found that bruxing in a molar restoration and excessive lateral excursive forces in a premolar restoration led to failure.[37] In a separate report, on four restorations, failure was ultimately due to design deficiencies and hyperocclusion.[35] For two of the four restorations, a Cerestore incisor and In-Ceram premolar, wear facets were found to be the sites of fracture origin. The remaining two crowns, failed due to design flaws.

Not all clinical failure origins are isolated to the porcelain veneer layer, as demonstrated in the above examples.[36] In a publication focusing on three all-ceramic restorations, fractographic evaluation determined stress build-up in the core materials ultimately leading to failure.

Clinical evidence suggests that *in situ* crown failure does not occur from point occlusal contacts, which are typical in laboratory studies, but rather that complex stress systems develop within the restorations. These crack systems typically develop anywhere within a restoration and propagate in random directions leading to failure.

Fractographic Analysis

Fracture in materials occurs in one of two ways: brittle or ductile. All-ceramic restorations fail by brittle fracture, alternatively described as failure without plastic deformation.[37] A method exists whereby brittle fracture in dental porcelains may be analyzed and the origin and direction of crack propagation (DCP) identified.[38] This technique is known as fractography, and when applied in failure analysis serves to clarify stress states at time of fracture. The restorations in Table 2.1 were fractographically evaluated with the use of light stereomicroscopy and scanning electron microscopy in an effort to determine the events leading to failure. With the use of this technique it has been determined that no one stress state governs clinical failure.

Table 2.1: Etiologies of Failure Found in Clinically Failed Restorations

Study	Restorations	Tooth	Type of restoration	Etiology of Failure/Fracture Origin
Scherrer SS 2007[30]	Single Crown	Molar	Procera Alumina	Bruxism /Margin Area
Scherrer SS 2007[30]	Single Crown	Premolar	In-Ceram Zirconia	Excursive Contact/Occlusal Surface
Scherrer SS 2006[35]	Single Crown	Incisor	Cerestore	Wear Facets/Occlusal Surface
Scherrer SS 2006[35]	Single Crown	Premolar	In-Ceram	Wear Facets/Occlusal Surface
Scherrer SS 2006[35]	Single Crown	Molar	Cerestore	Premature Contact/Occlusal Surface
Scherrer SS 2006[35]	Single Crown	Molar	PFM	Premature Contact/Occlusal Surface
Quinn JB 2005[36]	Single Crown	Molar	Procera AllCeram	Margin failure/Fracture Origin within thinnest portion of core material
Quinn JB 2005[36]	Single Crown	Molar	Cerestore Alumina-Spinel	Margin failure/Fracture Origin within thinnest portion of core material
Quinn JB 2005[36]	Single Crown	Incisor	Empress 2	Margin failure/Fracture Origin within thinnest portion of core material

Study Aim: Comparison of In Vitro & In Vivo Stress States at Failure

The aim of this study is to determine whether zirconia based all-ceramic restorations loaded-to-failure and fatigue tested develop the same random stress states at failure as do clinically failed restorations. The null hypothesis is that *in vitro* data could be correlated with clinical behavior only if stress states at failure are similar between restorations failed in the laboratory and those failing in the oral environments. It has previously been shown that higher energy stress states are present during failure in laboratory models, energy levels that are not found in situ.[40] However, a complete map of the stress states found in *in vitro* models for load to failure and fatigue testing remains to be outlined.[9]

Materials & Methods

Two groups of samples were fabricated for testing. The first for single-load-to-failure (SLF) and the second for fatigue testing (FT). For the SLF testing cohort, 5 groups of 10 samples were designed and fabricated (Table 2.2). Each group consisted of samples with identical coping thicknesses and varying occlusal porcelain thickness. For the FT testing cohort, 10 samples identical to the T1.75 group were selected from an ongoing FT study for optical imaging and SEM analysis. Test samples were fabricated from milled dies, milled zirconia copings and printed direct pressing resin patterns (Figure 6).

Table 2.2: Test Samples Coping & Veneer Thickness

Group	# Samples per Group (N)	Coping thickness (mm)	Occlusal Porcelain Thickness (mm)
T.55	10	0.4	0.55
T1.15	10	0.4	1.15
T1.75	10	0.4	1.75
T2.35	10	0.4	2.35
T2.95	10	0.4	2.95

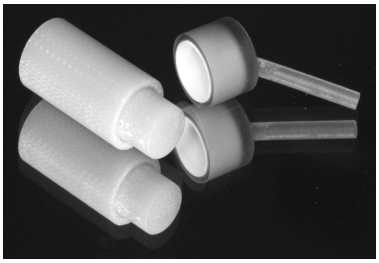

Figure 6. Die, DPRP & coping (inside DPRP)

Dies

3D CAD software, SolidWorks® (Dassault Systemes Solidworks Corp., Concord, MA), was used to design dies with the following dimensions (figure 7, Table 2.3):

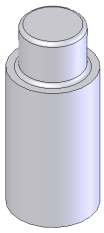

Figure 7. Die

Table 2.3: Die Dimensions

Parameter	Length(mm)
Total Height	25.05
Base Height	19.05
Core Height	6.0
Core Diameter	8.0
Total Diameter	11.0
Should Width	1.5
Occluso-Axial Bevel	0.5
Axio-Gingival Bevel	0.5
Axial Wall Taper	0^0 (degree)

Core height and shoulder width were loosely modeled on average dimensions of a prepared mandibular first molar for an all-ceramic restoration[39]. A continuously woven glass fabric epoxy resin laminate (National Electrical Manufacturers Association (NEMA) grade G10, Rosslyn, VA), was used as a milling substrate and has previously been reported in laboratory use[19,40]. Axio-occlusal and axio-gingival line angles were beveled 0.5 mm in order to prevent sharp line angles.

Copings

50 uniform thickness Lava™ Zirconia (3M ESPE, St. Paul, MN) copings were fabricated. Non-anatomic, cylindrically shaped designs were used in order to prevent

non-uniform stress distribution[20,21]. The cylindrical design should not be misconstrued as a standardized crown.

Direct Pressing Resin Patterns (DPRP)

DPRPs were used for application of IPS e.max Zirpress (Ivoclar Vivadent, Amherst, NY), in a manner similar to the lost wax technique (Figure 8), to LAVA™ zirconia (3M ESPE, St. Paul, MN) copings. Clear IPS e.max Ceram Zirliner (Ivoclar Vivadent, Amherst, NY) was applied to each coping, with firing and pressing guidelines obtained from the IPS e.max Zirpress Instructions for Use Manual (Table 2.4). High translucency, shade A1 IPS e.max Zirpress (Ivoclar Vivadent, Amherst, NY), ingots were used in order to facilitate optical imaging for subsequent fractographic analysis of failed restorations.

Figure 8. DPRP (Note sprue emerging from occlusal surface)

DPRPs were designed with 3D CAD software, SolidWorks® (Dassault Systemes Solidworks Corp., Concord, MA) and printed (Invision HR, 3D Systems Rock Hill, SC) using Visijet SR200 Blue, a polymer acrylic frequently used to cast jewelry. Clear IPS e.max glaze (Ivoclar Vivadent, Amherst, NY) was applied to each sample and fired

according to the manufacturer's recommendations (Table 2.4). Crowns were cemented with RelyX Luting Cement (3M ESPE, St Paul, MN) and aged in water for 30 days at 37°C in an incubator. Aging in this manner allows for chemically assisted crack growth[41].

Table 2.4: Press/Firing Parameters* for IPS e.max

IPS e.max	B (□C/□F)	S min	t ↗ (□C/□F)	T (□C/□F)	H min	V_1 (□C/□F)	V_2 (□C/□F)
ZirLiner	403/757	4:00	60/108	960/1760	1:00	450/842	959/1758
ZirPress (200g)	700/1292	NA	60/108	910/1670	15	500/932	910/1670
Glaze	403/757	6:00	60/108	770/1418	1:00-2:00	450/842	769/1416

***Table 2.5: Legend Table 2-4**

Porcelain Firing Table Parameters	Symbol
Start Temperature (^{0}C or ^{0}F)	B
Dry Time (min)	S
Temperature Rise	T ↗
Final Temperature	T
Hold Time	H
Vacuum Engage	V_1
Vacuum Disengage	V_2

Loading

Samples were failed in a universal testing machine (Model 5566 Instron, Acton, MA, USA) and electrodynamic fatigue unit (ELF 3300, EnduraTec Division, Bose Corporation, Minnetonka, MN, USA), with all data values recorded in Newton force. For single load to failure, forces were applied through a 6.25 mm tungsten carbide indenter at a rate of 1 mm/min. Samples fatigue tested, were loaded with a 6.25 mm tungsten carbide indenter, and failed between 380,000 cycles at 200 N and 470,000 cycles at 385

N. Samples were viewed under a stereomicroscope (MZ APO, Leica Microsystems Inc. Bannockburn, IL, USA) for determination of areas of interest with subsequent fractographic analysis using scanning electron micrographs (Hitachi S-3500N, Hitachi High-Technologies Europe GmbH, Krefeld, Germany).

Statistical Analysis

To test the hypothesis, a one-way ANOVA with standardized range test for pair-wise comparisons was considered. Assumptions of this test included: the subjects were randomly assigned to one of 5 groups and were independent of one another; the data within each group (each with a sample size of 10) were normally distributed with equal variances across groups; and residuals were normally distributed. Assumptions of normality within each group were verified with Q-Q plots and homogeneity of variance verified by Levene's test (P=.10). Tukey's studentize range test for multiple comparisons of force at failure amongst all possible pairings of groups was performed.

Results

Statistical Analysis Results

Thickness was represented as T.55, T1.15, T1.75, T2.35, and T2.95 (see Table 2.6) in the categorical variable group. Each group thickness value has 10 load (force at failure, Newton) values, for a total of 50 load values.

Table 2.6 outlines the loads at failure for groups T.55 through T2.95. With increasing porcelain thickness, the loads to failure similarly increased. Graphical display, one-way ANOVA and load comparisons are found in the visual display and tables 2.7 and 2.8.

Table 2.6: Analysis Variable : load (Force at Failure; Newton)

Group	N	Mean	Std Dev	Minimum	Maximum
T.55	10	1110.5	178.8	825.7	1293.9
T1.15	10	1568.8	343.6	913.5	2174.7
T1.75	10	1771.3	446.7	916.5	2338.1
T2.35	10	1988.5	595.2	821.8	2723.5
T2.95	10	2005.5	548.8	1044.0	2624.2

Visual Display for Descriptive Statistics for Load to Failure (Newton) Separated by Group

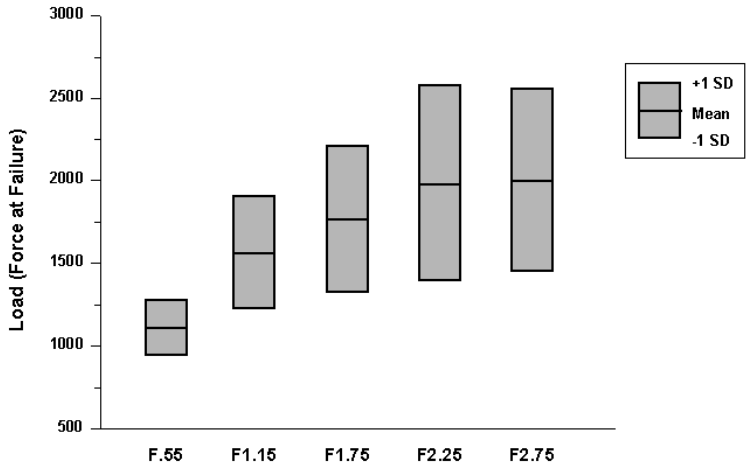

Table 2.7: One-Way ANOVA: Dependent Variable = load (Newton)

Source	DF	Sum of Squares	Mean Square	F Value	Pr > F
Model	4	5457654.77	1364413.69	6.79	0.0002
Error	45	9045107.43	201002.39		
Corrected Total	49	14502762.2			
R-Square	Coeff Var	Root MSE	Load Mean		
0.37	26.55	448.33	1688.9		

Table 2.8: Comparisons of Loads (Newton) at Failure between Thickness Groups

Group Comparison	Difference Between Means	Simultaneous 95% Confidence Limits		
T.55 – T1.15	-458.3	-1028.0	111.4	
T.55 – T1.75	-660.9	-1230.6	91.1	***
T.55 – T2.35	-878.0	1447.7	308.3	***
T.55 - T2.95	-895.0	1464.7	325.3	***
T1.15 – T1.75	-202.6	-772.3	367.1	
T1.15 – T2.35	-419.7	-989.4	150.0	
T1.15 – T2.95	-436.7	-1006.4	133.0	
T1.75 – T2.35	-217.1	-786.9	352.6	
T2.35 – T2.95	-17.0	586.7	-552.7	

Comparisons significant at the 0.05 level are indicated by ***

Checking the assumption of normally distributed data within groups the conclusion was that the distributions of force at failure for each group appear to be distributed normally. Levene's test shows at the 0.05 level, there is no shift in variation, and thus the data is homogeneous with respect to variation and the assumption of equal variance across groups is valid. Given the test statistic F = 6.79 with statistically significant p=0.0002, one can reject the null hypothesis and conclude that force at failure is dependent on thickness and appears to increase in the order of the following groups: T.55, T1.15, T1.75, T2.35, and T2.95. Statistically significant differences were found

between T.55 and T1.75; between T.55 and T2.35; and between T.55 and T2.95. The average load to failure was statistically different among the 5 thickness groups (P<.001). The average load to failure increased as the thickness of porcelain increased. From the pair-wise comparisons, T.55 was significantly different from T1.75, T2.35 and T2.95.

Fractographic Analysis

Table 2.9 outlines terms and definitions to be used for fractographic analysis of failed ceramic restorations.

Table 2.9: Terms & Definitions of Fractographic Patterns

Terms	Definitions
Hackle[α]	Are lines on the surface running in the local direction of cracking, separating parallel, but noncoplanar portions of the crack surface. Hackle lines are commonly formed when the crack moves rapidly.
Wake Hackles[α]	Is a hackle mark extending from a singularity at the crack front in the direction of cracking. It is created by the crack front advancing along the side of the singularity (eg: pore) before continuing on slightly different plane. Thus, wake hackle markings are excellent indicators of the direction of crack propagation.
Twist Hackle[α]	Markings that separate portions of the crack surface, each of which had rotated from the original crack plane in response to a lateral rotation or twist in the axis of principal tension. The roughly parallel segments point in the direction of local crack propagation.
Arrest Lines[α]	Is a sharp line on the fracture surface defining the crack front shape of an arrest or momentarily hesistated crack prior to resumption or crack propagation under a more or less altered stress configuration. Arrest lines are also indicators of the direction of crack propagation as the beginning of a crack event is always located on the concave side of the first arrest line.
Hertzian Cone Crackβ	Blunt impacts or blunt contact loading produce round Hertzian Cone Cracks. These may be complete or partial rings. The cone crack initiates as a ring just outside the footprint of the two contacting bodies. The size of the contact area depends upon the load, geometries, and elastic properties of the two materials.

α: Taken directly from Scherrer SS, Quinn GD, Quinn JB, Dent Mat 2008;24:1107-1113
β: Taken directly from Quinn GQ, Fractography of Ceramics and Glasses, NIST Publication 960-16 2007 p6-23

Single-Load-to-Failure Testing: Fractographic Analyses

The following figures describe the results of the fractographic analyses undertaken for the restorations that underwent load to failure testing in a universal testing machine.

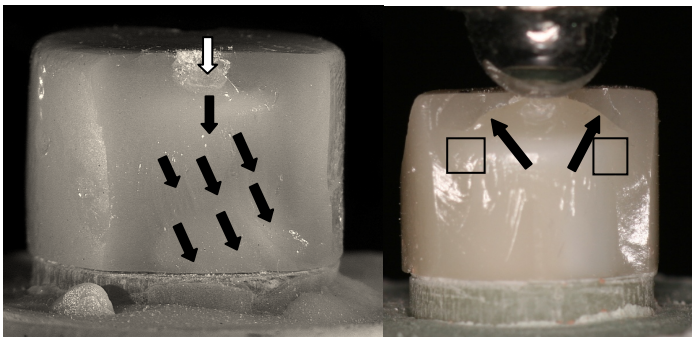

Figures 9 & 10:

Fig 9: Optical image (10X) of fracture origin and direction of crack propagation (DCP) generated from the occlusal surface (arrows). Fig 10: Optical image (10X) of Hertzian cone cracks indicated by arrows. Note spherical indenter seen on occlusal surface. (Boxes in fig 10: see fig11)

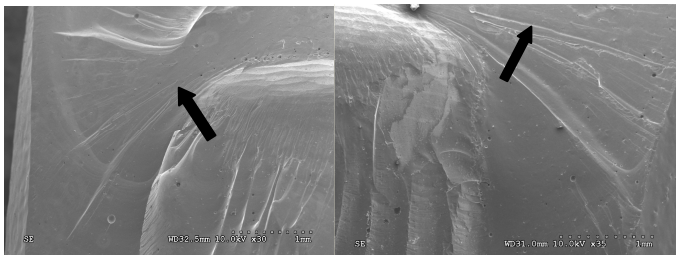

Figure 11:

SEMs of wake hackles, resulting from high loads at failure (arrows, see box fig. 10 for area outlined here).

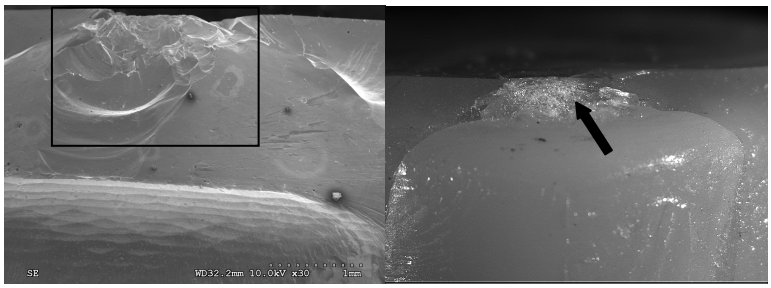

Figures 12 & 13:

Fig 12: SEM of contact damage: large numbers of fragments developed during SLF (area in rectangle). Fig 13: Optical image (10X) of contact damage: crushing damage accompanied by formation of powder-like debris (arrow). Area outlined is that found below an indenter; see fig 10 as example.

Fatigue Testing: Fractographic Analyses

The following figures describe the results of the fractographic analyses undertaken for the restorations that underwent fatigue testing in an electrodynamic fatigue unit.

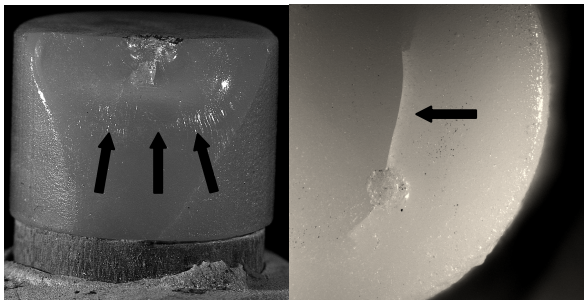

Figures 14 & 15:

Fig 14: Fracture origin and direction of crack propagation (DCP). Note: Twist Hackles (arrows). Fig 15: Hertzian cone cracks, occlusal view.

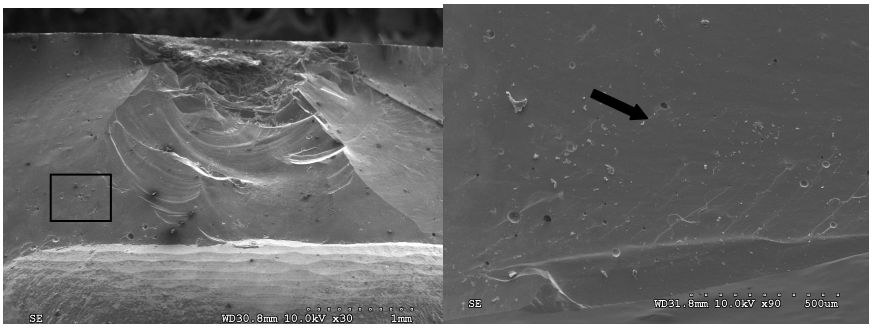

Figures 16 & 17:

Fig 16: Contact damage: large number of fragments generated. SEM at left is view defined by black box on right. Fig. 17: Wake hackle (arrow). Note area in black box found in fig 16 is the area seen here.

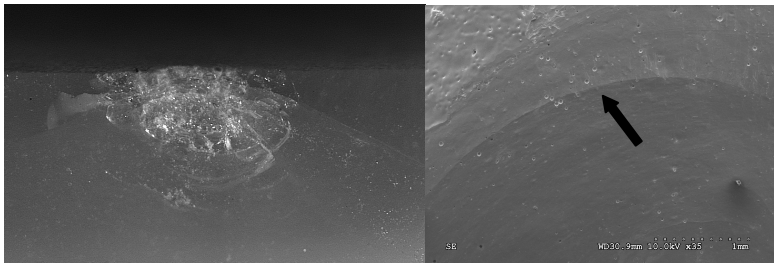

Figures 18 & 19:

Fig 18: Contact damage: crush zone – with powder-like debris formed (area outlined is that found below an indenter; see fig 10 as example). Fig 19: Arrest line: indicates interruption in crack front propagation.

Discussion

Fractographic analysis is undertaken to determine the causes or factors that have led to an undesired loss of function. In order for there to be a corollary between *in vitro* and *in vivo* data results, samples tested in the laboratory environment must fail in a manner similar to that found in the oral cavity.[33] As such, the samples tested in this study should exhibit the same fractographic patterns and failure mechanism seen from samples analyzed *in situ* to qualify for correlation.

Figures 9 and 14 are samples loaded-to-failure and fatigued to failure, respectively. These two samples are representative of their testing cohorts. In all samples from both testing methodologies failure origin was at the site of indenter contact, and the directions of crack propagation (DCP) where found to stem from these areas. This is in contrast with fractographic analysis of clinically failed restorations. In the clinical environment failure origin is often found elsewhere than the site of load application.[33] In both SLF and FT cohorts, wake hackles (See Table 2.9, Terms and Definition of fractographic patterns) are seen fanning out from the site of force delivery, indicating that fracture of the veneer layer stemmed from a wave front traveling occluso-cervically. As was previously discussed (see introduction) fractographic analyses has established the random nature of failure mechanisms encountered clinically. Those mechanisms do not result in a wave front propagating similar to that seen in the laboratory. Rather fracture origins are seen to develop at random and do not consistently travel in an occluso-cervical direction from occlusal origins of failure, as seen in the

laboratory. As such, failure origin and directions of crack propagation differ between laboratory and oral environments.

Among the samples tested in this study, the fractures found immediately adjacent to the sites of load application developed from blunt indentation stresses[33]. These fracture types are inconsistent with those found in clinically failed samples[40,41,42]. In the oral environment fracture origins are found at the cementation layer, margin area or occlusal surface (see table 2.1), rather than at the site of load application. In this study, all fracture origins were found at the site of load application, and stresses at these sites resulted in Hertzian cone cracks (Figure 10. HCC). This type of crack system is inconsistent with that found in the clinical arena[39]. The relevance of HCCs pertains to the type of force applied leading to failure. These types of systems are found with blunt indentation of test sample surface, the type of load resulting from a spherical indenter used in universal testing machines, and a type of loading not seen in the clinical environment[33].

Figures 11 and 17 demonstrate wake hackles found in both SLF and fatigue groups, respectively. These patterns develop as an advancing crack front encounters an elastic singularity, such as a pore or inclusion, split, circumvent the obstacle and re-emerge on the distal end. Generally, wake hackles provide the local direction of crack propagation. Figure 11 shows a representative wake hackle found among the load-to-failure cohort. Unlike those found in clinical samples, those found in the SLF group were, on average, much longer than those seen clinically. The significance of this finding relates to the magnitude of load application. With higher intensity loads wake hackles will demonstrate longer wakes. Clinically, these fracture patterns are typically much

shorter than those found *in vitro*, and reflect the lower Newton force applied. The wake hackles found in the fatigue groups were more clinically relevant, with lengths more comparable to *in vivo* samples, and reflect the forces generated between the *in situ* and fatigue testing environments. Equally, much like the twist hackles previously described, wake hackles provide insight into the direction of crack propagation and fracture origin. In all *in vitro* samples, the direction of wake hackle formation confirmed that the origin of crack propagation stemmed from the site of load application and not from elsewhere in the veneer layer; as is seen clinically.

Figures 12 and 17 are SEMs of fragmentation occurring immediately adjacent to sites of load application. What was characteristic with all laboratory samples was the number of fragments generated during failure. In the clinical arena a limited number is encountered, however as seen in these scanning electron micrographs, multiple fragments are generated during both SLF and fatigue testing. This is attributable to the high energy stress states generated in *in vitro* testing. The number of surfaces created is proportional to the energy applied.[33] This fact is exemplified in figures 16 and 18, where crush zones generate power-like debris. These findings indicate that high amounts of energy were stored and released during laboratory testing and are in contrast with reports of clinically failed restorations.[9] Crush zones are never encountered clinically.

Arrest lines (fig. 19) are sharp demarcations found on fracture surfaces where a temporary hesitation in crack front propagation is found.[5] Clinically, these fracture patterns are readily identified and are common[43]. None of the SLF samples exhibited these patterns, which denotes the continual and gradually increasing forces applied during

testing. Among the fatigued cohort, however, arrest lines were commonly and readily identified, a finding not entirely unexpected given the intermittent application of force[44]. These fracture patterns, and the lack thereof among the SLF cohort, highlight the different stress states generated in SLF testing and the clinical arena.

Clinical failure of ceramic and porcelain-fused-to-metal restorations is the result of occlusal loads generating random stress states leading to porcelain veneer fracture. This mode of failure was not found in either the SLF or FT samples tested in this study. In the laboratory environment wake hackles and twist hackles identified in test samples consistently demonstrated that the origin of failure and the direction of crack propagation radiated from the site of indenter loading. This failure mechanism in *in vitro* testing is in contrast to samples failing intraorally. Data from *in vitro* testing may only be correlated with *in vivo* performance if the stress states generated in both environments are comparable. At this time, there are no laboratory testing methods able to reliably generate failure in large numbers of test samples similar to that occurring *in situ*; therefore the null hypothesis is rejected.

Study Limitations

The geometry of the test samples used in this study do not reflect those found clinically. For a direct comparison of failure outcome, anatomically shaped laboratory samples would have better reflected stress states at failure than those used.

Each sample was aged for 30 days at 37ºC in order to induce chemically assisted crack growth. This time period is commonly used in the laboratory setting, however it is unknown to what length of time a sample requires aging[33].

The loads at failure encountered in this study are in excess of the loads typically encountered intraorally[33]. Previously reported ranges of Newton forces encountered clinically have been 9 to 180 and as high as 150 to 665[37, 45]. Even if the highest value reported (665N) is taken as standard the values reported in this study (1110.5-2005.N) for single load to failure are in excess to those found in the oral cavity. The Newton forces encountered in fatigue testing were more within acceptable limits (200-380N).

Conclusion

SLF and FT generate stress states at failure inconsistent with that found intraorally. Fractographic analysis of these *in vitro* testing models demonstrate an occlusally derived failure mechanism with the fracture origin and direction of crack propagation radiating from an area immediately adjacent to the site of indenter loading. Conversely, fractographic analysis of clinically failed restorations demonstrates fracture origin and direction of crack propagation typically stemming from the cementation layer, the restoration margin area or the occlusal surface.

References

1. Raigrodsky AJ. Contemporary All-Ceramic Fixed Partial Dentures: A Review. Dent Clin N Am 2004;48:531-544

2. Naylor WP. Introduction to Metal-Ceramic Technology 2nd Ed. Quintessence Books 2009

3. Korson D. Natural Ceramics. Quintessence Books 1990

4. Al-Amleh B, Lyons K, Swain M. Review Article Clinical Trials in Zirconia: A Systematic Review. J Oral Rehabil 2010;37(8):641-52

5. Denry I, Kelly JR. State of the Art of Zirconia for Dental Applications. Dent Mat 2008;24:299-307

6. Christensen GJ. Porcelain-Fused-to-Metal Versus Zirconia-Based Ceramic Restorations. JADA 2009;140:1036-39

7. Speer FM. The Risk of the Metal Free Practice. J Esthet Restor Dent 2009;21(2):71-4

8. Phillips RW, Science of Dental Materials 9th Ed., W.B. Saunders Company, 1991, p.13-19, p.54-55

9. Aboushelib MN, Feilzer AJ, de Jager N, Kleverlaan CJ. Bridging the Gap Between Clinical Failure and Laboratory Fracture Strength Tests Using a Fractographic Approach. J Biomed Mater Res Part B: Appl Biomater 2008;87B:139-145

10. Craig RG, Powers JM Restorative Dental Materials 11th Ed, Mosby 2002, p.52

11. Twiggs SW, Mackert JR, Oxford AL, Ergle JW, Lockwood PE. Isothermal Phase Transformations of a Dental Porcelain. Dent Mat 2005;21:580-84

12. Incropera FP, DeWitt DP Fundamentals of Heat & Mass Transfer 5th, Wiley 2002, p.59

13. Hisbergues M, Vendeville S, Vendeville P. Zirconia: Established Facts and Perspective for a Biomaterial in Dental Implantology. J Biomed Mater Res Part B: Appl Biomater 88B: 519-529, 2009

14. Bisson JF, Fournier D, Poulain M, Lavigne O, Mevrel R. Thermal Conductivity of Yttria-Zirconia Single Crystals, Determined by Spatially Resolved Infrared Thermography. J Am Ceram Soc 2000;83(8):1993-98

15. Swain MV. Unstable Cracking (Chipping) of Veneering Porcelain on All-Ceramic Dental Crowns and Fixed Partial Dentures. Acta Biomaterialia 2009;5(5):1668-77

16. Benetti P, Bona AD, Kelly JR. Evaluation of Thermal Compatility between core and veneer dental ceramics using shear bond strength test and contact angle measurement Dent Mat 2010 Epub

17. Goodacre CJ, Campagni WV, Aquilino SA. Tooth Preparations for Complete Crowns: An Art Form Based on Scientific Principles. J Prosthet Dent 2001;85:363-76

18. Wang Y, Katsube N, Seghi RR, Rokhlin SI. Statistical Failure Analysis of Adhesive Resin Cement Bonded Dental Ceramics. Engineering Fracture Mechanics 2007;74:1838-56

19. Kelly JR. Development of a Clinically Validated Bulk Failure Test for Ceramic Crowns. J Prosthet Dent 2010;104:228-238

20. Scherrer SS, de Rijk WG. The Effect on Crown Length on the Fracture Resistance of Posterior Porcelain and Glass-Ceramic Crowns. Int J Prosthodont 1992;5:550-57

21. Kelly JR, Tesk JA, Sorensen JA. Failure of All-Ceramic Fixed Partial Dentures In Vitro and In Vivo: Analysis and Modeling. J Dent Rest 1995;74(6):1253-58

22. Dehoff P, Barrett AA, Lee RB, Anusavice KJ. Thermal Compatibility of Dental Ceramic Systems Using Cylindrical and Spherical Geometries. Dent Mat 2008;24:744-52

23. Guazzato M, Walton TR, Franklin W, Davis G, Bohl C, Klineberg I. Influence of Thickness and Cooling Rate on Development of Spontaneous Cracks in Poreclain/Zirconia Structures. Aust Dent J 2010;55:306-310

24. Taggart WH. A New and Accurate Method of Making Gold Inlays. Dent Cosmos 1907(49); 111-7, 121

25. Charles RJ, Hillig WB. The Kinetics of Glass Failure by Stress Corrosion. J Appl Physiol 1958;29:1549-53

26. Mjor IA. Minimum Requirements for New Dental Materials. J Oral Rehab 2007;34:907-912

27. Quinn GD, Fractography of Ceramics and Glasses, NIST Special Publication 960-16 2007: Chapter 7

28. Fréchette VD, Michalske TA. Failure Analysis of Brittle Materials. Bull Amer Ceram Soc 1978;57(4)427-429

29. Quinn GD, Fractography of Ceramics and Glasses, NIST Special Publication 960-16: Chapter 7, p.7-63

30. Scherrer SS, Quinn JB, Quinn GD, Wiskott HWA. Fractographic Ceramic Failure Analysis Using the Replica Technique. Dent Mat 2007;23:1397-1404

31. Callister WD, Materials Science & Engineering an Introduction 6th Ed, John Wiley & Sons, Inc 2003; p.2-5

32. Mjor IA. Practice Based Dental Research. J Oral Rehab 2007;34:913-920

33. Kelly JR. Clinically Relevant Approach to Failure Testing of All-Ceramic Restorations. J Prosthet Dent 1999;81:652-61

34. Scherrer SS, Quinn GD, Quinn JB. Fractographic Failure Analysis of a Procera AllCeram Crown Using Stereo and Scanning Electron Microscopy. Dent Mat 2008;24:1107-1113

35. Scherrer SS, Quinn JB, Quinn GD, Kelly JR. Failure Analysis of Ceramic Clinical Cases Using Qualitative Fractography. Int J Prosthodont 2006;19:185-192

36. Quinn JB, Quinn GD, Kelly JR, Scherrer SS. Fractographic Analysis of Three Ceramic Whole Crown Restoration Failure. Dent Mat 2005;21:920-929

37. Craig RG, Restorative Dental Materials 11th Ed, Mosby 2002

38. Quinn GQ, Fractography of Ceramics and Glasses, NIST Publication 960-16 2007

39. Quinn GQ, Fractography of Ceramics and Glasses, NIST Publication 960-16 2007 p10-34

40. Kelly JR, Campbell SD, Bowen HK. Fracture-Surface Analysis of Dental Ceramics. J Prosthet Dent 1989;62:536-41

41. Thompson JY, Anusavice KJ, Naman A, Morris HF. Fracture Surface Analysis Characterization of Clinically Failed All-Ceramic Crowns. J Dent Res 1994;73:1824-32

42. Kelly JR, Giordano R, Pober R, Cima MJ. Fracture Surface Analysis of Dental Ceramics: Clinically Failed Restorations. Int J Prosthodont 1990;3:430-40

43. Taskonak B, Mecholsky JJ, Anusavice KJ, Fracture Surface Analysis of Clinically Failed Fixed Partial Dentures. J Dent Res 2006;85:277-81

44. Bayne SC. Dental Restorations for Oral Rehabilitation - Testing of Laboratory Properties Versus Clinical Performance for Clinical Decision Makin. J Oral Rehabil 2007;34:921-932

45. DeLong R, Douglas WH. Development of an artificial oral environment for the testing of dental restoratives: bi-axial force and movement control. J Dent Res 1983; 62: 32-6